



Full Text View

[Volume 29, Issue 9 \(September 1999\)](#)

Journal of Physical Oceanography

Article: pp. 2318–2331 | [Abstract](#) | [PDF \(248K\)](#)

Stability Regimes of Finite Depth Short-Crested Water Waves

Mansour Ioualalen

Laboratoire d'Océanographie Dynamique et de Climatologie, Paris, France

Christian Kharif

Institut de Recherche sur les Phénomènes Hors Equilibre, Laboratoire IOA, Marseille, France

Anthony J. Roberts

Department of Mathematics and Computing, University of Southern Queensland, Toowoomba, Australia

(Manuscript received February 10, 1998, in final form October 22, 1998)

DOI: 10.1175/1520-0485(1999)029<2318:SROFDS>2.0.CO;2

ABSTRACT

Stability regimes of three-dimensional surface gravity waves are provided in this study. The stability regimes for waves in water of finite depth differ significantly from those for waves in deep water. In particular, these waves are no longer unstable to phase-locked horseshoe-patterned disturbances, and the perturbed wave fields have more complex geometry than those in deep water. It is also shown that there is a critical restabilization value of the depth parameter below which the timescales of the surface wave variations shorten exponentially. This critical value depends on the wave steepness and the degree of three-dimensionality of the unperturbed wave field. Finally, it is predicted that these waves are quasi-observable.

1. Introduction

Short-crested waves are defined as doubly periodic wave patterns in both horizontal directions. They can be generated by the reflection of a two-dimensional progressive wave from a sea wall, where there is angle θ between the incident direction and the normal to the wall (y direction). These waves are symmetrical about the sea wall and assumed to be monophasic propagating along the wall (x direction). They are the genus three-dimensional wave patterns and their study is the first step to approach the physics of the wide range of uninvestigated three-

Table of Contents:

- [Introduction](#)
- [Mathematical formulation](#)
- [Numerical results and](#)
- [REFERENCES](#)
- [APPENDIX](#)
- [TABLES](#)
- [FIGURES](#)

Options:

- [Create Reference](#)
- [Email this Article](#)
- [Add to MyArchive](#)
- [Search AMS Glossary](#)

Search CrossRef for:

- [Articles Citing This Article](#)

Search Google Scholar for:

- [Mansour Ioualalen](#)
- [Christian Kharif](#)
- [Anthony J. Roberts](#)

dimensional water waves. The study of three-dimensional wave fields is suitable to obtain a more realistic description of the ocean surface. These waves admit two two-dimensional limits, $\theta = 0^\circ$ and $\theta = 90^\circ$, corresponding respectively to normally reflected standing waves and progressive Stokes waves.

[Roberts \(1983\)](#) pointed out harmonic resonances introduced by the three-dimensionality. The perturbation series he used has formally an everywhere zero-radius of convergence because high harmonics interact through resonances with the fundamental modes acting as a forcing propagating at the same frequency. Taking advantage of this work, [Ioualalen and Kharif \(1993, hereafter IK93\)](#) studied the stability of deep water short-crested waves to superharmonic disturbances in order to measure the timescales of these resonances. They identified the associated instabilities as [McLean's \(1982a\)](#) class I instabilities and found that they are very sporadic and weak (long timescale evolution). This is why the authors qualified these waves as "quasi-observable." [Ioualalen and Kharif \(1994, hereafter IK94\)](#) confirmed this result by comparing superharmonic instabilities to subharmonics and found that timescales of harmonic resonances are at least two h -order longer than timescales of subharmonic instabilities, where h is the wave steepness ($h < 1$).

IK94 proposed a classification of the different instabilities involved in such a wave field by introducing subclasses of classes I and II described by [McLean \(1982a\)](#). Like Stokes two-dimensional progressive waves, they are unstable to class Ia unidirectional modulational perturbations [e.g., [Benjamin and Feir \(1967\)](#) and [Zakharov \(1968\)](#)]. Later, [Kimmoun et al. \(1999\)](#) found like [McLean \(1982a\)](#) that for a wave steepness larger than approximately $h = 0.32$ the dominant instabilities of progressive waves "close" to the Stokes wave limit (for $\theta = 80^\circ$) are three-dimensional, belong to class II, and are phase-locked with the basic wave. Critical values of h , for which class I instabilities stop dominating, depend on angle θ (IK94). Similarly to Stokes waves, for wave steepnesses weaker than this critical value, class Ia subharmonic instabilities dominate and are two-dimensional (IK94). For waves close to the standing wave limit [Kimmoun et al. \(1999\)](#) showed (for $\theta = 10^\circ$) that subharmonic class Ia instabilities dominate whatever is the wave steepness. Fully three-dimensional short-crested waves [[Kimmoun et al. \(1999\)](#) for $\theta = 40^\circ$] are more subject to class Ib instabilities, which grow more slowly than two-dimensional wave instabilities and modulate the wave train in the two horizontal directions. [Badulin et al. \(1995\)](#) using a Hamiltonian weakly nonlinear formulation explained these different stability regimes by interactions between the different classes of instability when they overlap each other.

As far as shallow short-crested water waves are concerned, experiments have been performed by [Hammack et al. \(1989\)](#) who suggested that these waves are observable over a certain time. [Ioualalen et al. \(1996\)](#) studied their stability to superharmonic perturbations in order to analyze their contribution. They found that these instabilities may be very strong (at least stronger than deep water modulational instabilities) for some particular flow geometries in contrast to deep water waves. They proposed a critical value of the nondimensional depth parameter $d = 1$ for which shallower water motion can be unobservable. They also showed that instabilities related to standing wave harmonic resonances ($\theta = 10^\circ$) [e.g., [Mercer and Roberts \(1994\)](#)] "contaminate" the whole three-dimensional wave field, with the exception of two-dimensional progressive waves, although their growth rates appear to be significant only for long-crested waves "close" to angle $\theta = 0^\circ$. However, they concluded that finite depth short-crested waves are generally observable because the strong superharmonic instabilities are localized in very narrow bands in the (d, θ) parameter regime.

In the present study we compute the general stability problem for weakly nonlinear finite depth short-crested waves in order to forecast which classes of instability are more likely to develop significantly and to compare their timescales to those of superharmonic instabilities and discuss their observability. We have limited our study to wave steepness $h = 0.23$ and depth $d = 1$ because beyond these values, we generally met difficulties in identifying the different instabilities involved. This is due to nonlinear interactions between classes of instability when they overlap: in practice, it has been found difficult to make a distinction between two different classes of instability when they have one interacting mode in common in their n -mode resonant interaction.

2. Mathematical formulation

We consider surface gravity waves on an inviscid, incompressible fluid of finite depth where the flow is assumed irrotational. The governing equations are

$$\Delta\phi = 0, \quad \text{for } -d < z < \eta(x, y, t), \quad (1)$$

$$\phi_z = 0, \quad \text{for } z = -d, \quad (2)$$

$$\phi_t + \eta + \frac{1}{2}(\phi_x^2 + \phi_y^2 + \phi_z^2) = 0, \quad \text{on } z = \eta(x, y, t), \quad (3)$$

$$\eta_t + \phi_x \eta_x + \phi_y \eta_y - \phi_z = 0, \quad \text{on } z = \eta(x, y, t), \quad (4)$$

where d is the depth of the fluid, $\Phi(x, y, z, t)$ is the velocity potential, and $z = \eta(x, y, t)$ is the equation of the free surface. Like [Hsu et al. \(1979\)](#), [Eqs. \(1\)–\(4\)](#) are given in dimensionless form with respect to the reference length $1/k$ and the reference time $(gk)^{-1/2}$, where g is the gravitational acceleration and k the wavenumber of the incident wave train. Let us define a frame of reference (x^*, y^*, z^*, t^*) so that $x^* = x - ct$, $y^* = y$, $z^* = z$, and $t^* = t$ where c represents the propagation speed of the wave train and is equal to ω/α , ω being the frequency of the wave and $\alpha = \sin(\theta)$ is the x -direction wavenumber, the y -direction wavenumber being $\beta = \cos(\theta)$. One can refer to [Hsu et al. \(1979\)](#) and [Roberts \(1983\)](#) for deep water or [Marchant and Roberts \(1987\)](#) for a complete description of the flow geometry. In this frame of reference (x^*, y^*, z^*, t^*) moving with the wave, the system of [Eqs. \(1\)–\(4\)](#) admits steady unperturbed solutions $\bar{\eta}(x, y)$ and $\bar{\Phi}(x, y, z)$ of the following form, where the asterisks are henceforth omitted for sake of simplicity:

$$\bar{\eta}(x, y) = \sum_{i=1}^{\infty} h^i \sum_{m,n} c_{i,mn} \cos(m\alpha x) \cos(n\beta y), \quad (5)$$

$$\begin{aligned} \bar{\phi}(x, y, z) = & -cx + \sum_{i=1}^{\infty} h^i \sum_{m,n} d_{i,mn} \sin(m\alpha x) \\ & \times \cos(n\beta y) \frac{\cosh[\gamma_{mn}(z + d)]}{\cosh(\gamma_{mn}d)}, \end{aligned} \quad (6)$$

$$\omega = \sum_{i=0}^{\infty} h^i \omega_i, \quad (7)$$

where $\gamma_{mn} = (m^2\alpha^2 + n^2\beta^2)^{1/2}$. The truncated solutions given by [Marchant and Roberts \(1987\)](#) represent doubly periodic Fourier series expansions in a small parameter h defined as the half of the nondimensional peak-to-trough height since the peak of the wave is fixed at $(x, y) = (0, 0)$; that is, $h = [\bar{\eta}(0, 0) - \bar{\eta}(\pi, 0)]/2$. These waves have been computed by [Marchant and Roberts \(1987\)](#) using the Padé approximation or Shanks transform to accelerate the convergence of the derived expansions. In the present study, solutions up to the 35th order have been computed. [Roberts \(1983\)](#) and [Marchant and Roberts \(1987\)](#) estimated the error involved in neglecting higher-order modes to be of order $h^{35/3}$; this is sufficient for our purpose since only low harmonics are involved in noticeable instabilities. The numerical convergence of the expansions is broadly discussed in [Marchant and Roberts \(1987\)](#) and [Ioualalen et al. \(1996\)](#). Moreover, the truncation of the expansions at reasonably high order is meaningful because for further modes, that is, high harmonics, dissipation processes (not considered here) dominate nonlinear processes. Like IK94, we define

$$\eta(x, y, t) = \bar{\eta}(x, y) + \eta'(x, y, t), \quad (8)$$

$$\phi(x, y, z, t) = \bar{\phi}(x, y, z) + \phi'(x, y, z, t), \quad (9)$$

where we assume that the surface elevation and the velocity potential are linear superpositions of a steady unperturbed wave $(\bar{\eta}, \bar{\phi})$ and infinitesimal unsteady perturbations (η', ϕ') so that $\eta' \ll \bar{\eta}$ and $\phi' \ll \bar{\phi}$. After substituting [\(8\)–\(9\)](#) expressions into [Eqs. \(1\)–\(4\)](#) and linearizing, we obtain the first-order perturbation equations

$$\text{on } z = \bar{\eta}(x, y). \quad (13)$$

Note that all local time derivatives of the unperturbed solutions $(\bar{\eta}, \bar{\phi})$ vanish in this new frame of reference propagating at the same wave speed as the unperturbed wave. We look for nontrivial solutions of [Eqs. \(10\)–\(13\)](#) of the form

$$\eta' = e^{-i\sigma t} e^{i(px+qy)} \sum_{J=-\infty}^{\infty} \sum_{K=-\infty}^{\infty} a_{JK} e^{i(J\alpha x + K\beta y)}, \quad (14)$$

$$\begin{aligned} \phi' &= e^{-i\sigma t} e^{i(px+qy)} \sum_{J=-\infty}^{\infty} \sum_{K=-\infty}^{\infty} b_{JK} e^{i(J\alpha x + K\beta y)} \\ &\times \frac{\cosh[\kappa_{JK}(z + d)]}{\cosh(\kappa_{JK}d)}, \end{aligned} \quad (15)$$

where $\kappa_{JK} = [(p + J\alpha)^2 + (q + K\beta)^2]^{1/2}$. If $p = N\alpha$ and $q = M\beta$ are integers (p and q are integer multiples of the main wavenumbers), the wavelengths in x direction and y direction of the perturbations are the same, respectively, as the longitudinal and the transversal wavelengths of the basic wave, and the perturbations are called superharmonic. If $p \neq N\alpha$ and $q \neq M\beta$, the perturbations contain components with wavelengths in the x direction and y direction greater than, respectively, the longitudinal and the transversal wavelengths of the basic wave, and the perturbations are called subharmonic. Mixed perturbations are also enabled. The stability analysis consists in determining coefficients a_{JK} , b_{JK} , and the set of eigenvalues σ . Since the system of [equations \(10\)–\(13\)](#) is real valued, the eigenvalues σ appear in complex conjugate pairs. Thus, an instability corresponds to $\mathbf{I}(\sigma) \neq 0$. For $h = 0$, the unperturbed wave is given by $\bar{\eta} = 0$ and $\bar{\phi} = -c_0 x$ with $c_0 = \omega_0/\alpha = \tanh^{1/2}(d)/\alpha$. Then the eigenvalues are $\sigma_{JK}^s(p, q) = -(p + J\alpha)c_0 + s[\kappa_{JK} \tanh(\kappa_{JK}d)]^{1/2}$ with $s = \pm 1$, $\text{sgn}[s\mathbf{I}(-i\sigma)]$ being the signature of the perturbation (e.g., [MacKay and Saffman 1986](#)). One can note the artificial degeneracy $\sigma_{JK}^s(p, q) = \sigma_{-i, K-j}^s(p + i\alpha, q + j\beta)$ introduced by [expressions \(14\)–\(15\)](#), which keeps the eigenmodes unchanged; eventually this allows us to consider only $0 \leq p \leq \alpha$ and $0 \leq q \leq \beta$. The real-valued set of eigenvalues $\{\sigma_{JK}^s\}$ causes the wave to be neutrally stable for $h = 0$. Instabilities arise as the wave steepness h increases. We use here the work of IK94 who took advantage of the useful work of [MacKay and Saffman \(1986\)](#) on Hamiltonian systems: we apply the necessary condition for instability in terms of collision of eigenvalues of opposite signatures (s) or at zero frequency. An instability can arise if for some wave steepness h , two modes have the same frequency; that is, $\sigma_{J_1 K_1}^s(p, q, h) = \sigma_{J_2 K_2}^{-s}(p, q, h)$. The derived condition for the waves considered is slightly different from the condition given by IK94 in their Eq. (2.12): the new condition explicitly takes the depth d as a parameter and recovers IK94 condition when d tends to infinity. The new condition takes the following form for $s = 1$ ($s = -1$ corresponds to an opposite direction of propagation):

$$[\kappa_{J_1 K_1} \tanh(\kappa_{J_1 K_1} d)]^{1/2} + [\kappa_{J_2 K_2} \tanh(\kappa_{J_2 K_2} d)]^{1/2} = (J_1 - J_2) \tanh^{1/2}(d). \quad (16)$$

We shall use here the same procedure as in IK94 to classify instabilities involved in such flows and use the same notation in terms of geometrical resonance conditions given by [Phillips \(1960\)](#), with our new condition [\(16\)](#).


a. Class Ia ($j = 1, K_1 = K_2 = 1$) or class Ia' ($j = 1, K_1 = K_2 = -1$)

Condition [\(16\)](#) becomes

$$\begin{aligned} &[(p + \alpha)^2 + (q + \beta)^2]^{1/4} \\ &\times \tanh^{1/2}\{d[(p + \alpha)^2 + (q + \beta)^2]^{1/2}\} \\ &+ [(p - \alpha)^2 + (q + \beta)^2]^{1/4} \\ &\times \tanh^{1/2}\{d[(p - \alpha)^2 + (q + \beta)^2]^{1/2}\} \\ &= 2 \tanh^{1/2}(d). \end{aligned} \quad (17)$$

In a coordinate system with center of symmetry, $P = p$ and $Q = q + \beta$, this equation is

$$\begin{aligned} & [(P + \alpha)^2 + Q^2]^{1/4} \tanh^{1/2}\{d[(P + \alpha)^2 + Q^2]^{1/2}\} \\ & + [(P - \alpha)^2 + Q^2]^{1/4} \tanh^{1/2}\{d[(P - \alpha)^2 + Q^2]^{1/2}\} \\ & = 2 \tanh^{1/2}(d). \end{aligned} \quad (18)$$

[Figure 1](#)  displays examples of linear resonance curves for various angles θ and depths d and the associated geometrical construction, where

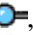

$$\mathbf{k}_1 = \mathbf{k}_2 + \mathbf{k}_{01} + \mathbf{k}_{02} \quad \text{and} \quad \omega'_1 = \omega'_2 + 2\omega'_0, \quad (19)$$

with $\mathbf{k}_1 = (p + \alpha, q + \beta)$, $\mathbf{k}_2 = (p - \alpha, q + \beta)$, $\mathbf{k}_{01} = \mathbf{k}_0^+ = (\alpha, \beta)$, and $\mathbf{k}_{02} = \mathbf{k}_0^- = (\alpha, -\beta)$. The frequencies in finite depth are

$$\omega'_1 = |\mathbf{k}_1|^{1/2} \tanh^{1/2}\{d[(p + \alpha)^2 + (q + \beta)^2]^{1/2}\}, \quad (20)$$

$$\omega'_2 = -|\mathbf{k}_2|^{1/2} \tanh^{1/2}\{d[(p - \alpha)^2 + (q + \beta)^2]^{1/2}\}, \quad (21)$$

$$\begin{aligned} \omega'_0 & = |\mathbf{k}_{01}|^{1/2} \tanh^{1/2}(d) = |\mathbf{k}_{02}|^{1/2} \tanh^{1/2}(d) \\ & = \tanh^{1/2}(d). \end{aligned} \quad (22)$$

Note that the symmetry of the resonance curves about the P and Q axes allows us to perform the numerical study for only $P \geq 0$ and $Q \geq 0$. For deep enough water ([Fig. 1](#) , $d = 2$) the shape of the curves is slightly different compared to the deep water case, while for shallower depths ([Fig. 1](#) , $d = 0.5$) the curves are strongly “compressed” with decreasing d . The curves tend to a fixed point ($p = q = 0$) when d tends to zero due to the bed conditions [[2](#)] and [[11](#)] although our formulation must be replaced by shallow water equations for very small values of d .

b. Class Ib ($j = 1, K_1 = 1, K_2 = -1$) or class Ib' ($j = 1, K_1 = -1, K_2 = 1$)

Condition [\(16\)](#) becomes

$$\begin{aligned} & [(p + \alpha)^2 + (q + \beta)^2]^{1/4} \\ & \times \tanh^{1/2}\{d[(p + \alpha)^2 + (q + \beta)^2]^{1/2}\} \\ & + [(p - \alpha)^2 + (q - \beta)^2]^{1/4} \\ & \times \tanh^{1/2}\{d[(p - \alpha)^2 + (q - \beta)^2]^{1/2}\} \\ & = 2 \tanh^{1/2}(d). \end{aligned} \quad (23)$$

In a coordinate system with center of symmetry, $P = p\alpha + q\beta$ and $Q = -p\beta + q\alpha$, the equation becomes symmetrical:

$$\begin{aligned} & [(P + 1)^2 + Q^2]^{1/4} \tanh^{1/2}\{d[(P + 1)^2 + Q^2]^{1/2}\} \\ & + [(P - 1)^2 + Q^2]^{1/4} \tanh^{1/2}\{d[(P - 1)^2 + Q^2]^{1/2}\} \\ & = 2 \tanh^{1/2}(d). \end{aligned} \quad (24)$$

Similarly, in [Fig. 2](#)  we have

$$\mathbf{k}_1 = \mathbf{k}_2 + 2\mathbf{k}_{01} \quad \text{and} \quad \omega'_1 = \omega'_2 + 2\omega'_0, \quad (25)$$

with $\mathbf{k}_1 = (p + \alpha, q + \beta)$, $\mathbf{k}_2 = (p - \alpha, q - \beta)$, and $\mathbf{k}_{01} = \mathbf{k}_0^+ = (\alpha, \beta)$,

$$\omega'_1 = |\mathbf{k}_1|^{1/2} \tanh^{1/2}\{d[(p + \alpha)^2 + (q + \beta)^2]^{1/2}\}, \quad (26)$$

$$\omega'_2 = -|\mathbf{k}_2|^{1/2} \tanh^{1/2}\{d[(p - \alpha)^2 + (q - \beta)^2]^{1/2}\},$$

$$\omega'_0 = \tanh^{1/2}(d). \quad (27)$$

c. Class IIa ($j = 1, K_1 = 1, K_2 = 2$) or class IIa' ($j = 1, K_1 = -1, K_2 = -2$)

Condition (16) becomes

$$\begin{aligned} & [(p + \alpha)^2 + (q + \beta)^2]^{1/4} \\ & \times \tanh^{1/2}\{d[(p + \alpha)^2 + (q + \beta)^2]^{1/2}\} \\ & + [(p - 2\alpha)^2 + (q + 2\beta)^2]^{1/4} \\ & \times \tanh^{1/2}\{d[(p - 2\alpha)^2 + (q + 2\beta)^2]^{1/2}\} \\ & = 3 \tanh^{1/2}(d). \end{aligned} \quad (28)$$

For this class the axes of symmetry are

$$\begin{aligned} P &= \frac{p\alpha - (1/3)q\beta - (4/9)\beta^2}{1 - (8/9)\beta^2} \quad \text{and} \\ Q &= \frac{-q\alpha + (1/3)p\beta - (4/3)\alpha\beta}{1 - (8/9)\beta^2}. \end{aligned} \quad (29)$$

The resonance condition under in these variables becomes, with $A = 1 - (8/9)\beta^2$,

$$\begin{aligned} & [(P + 1)^2 + Q^2]^{1/4} \tanh^{1/2}\{d[(P + 1)^2 + Q^2]^{1/2}A^{1/2}\} \\ & + [(P - 2)^2 + Q^2]^{1/4} \tanh^{1/2}\{d[(P - 2)^2 + Q^2]^{1/2}A^{1/2}\} \\ & = 3 \tanh^{1/2}(d)/A^{1/4}. \end{aligned} \quad (30)$$

Similarly, in Fig. 3 we have

$$\mathbf{k}_1 = \mathbf{k}_2 + \mathbf{k}_{01} + 2\mathbf{k}_{02} \quad \text{and} \quad \omega'_1 = \omega'_2 + 3\omega'_0, \quad (31)$$

with $\mathbf{k}_1 = (p + \alpha, q + \beta)$, $\mathbf{k}_2 = (p - 2\alpha, q + 2\beta)$, $\mathbf{k}_{01} = \mathbf{k}_0^+ = (\alpha, \beta)$, and $\mathbf{k}_{02} = \mathbf{k}_0^- = (\alpha, -\beta)$.

$$\omega'_1 = |\mathbf{k}_1|^{1/2} \tanh^{1/2}\{d[(p + \alpha)^2 + (q + \beta)^2]^{1/2}\}, \quad (32)$$

$$\omega'_2 = -|\mathbf{k}_2|^{1/2} \tanh^{1/2}\{d[(p - 2\alpha)^2 + (q + 2\beta)^2]^{1/2}\},$$

$$\omega'_0 = \tanh^{1/2}(d). \quad (33)$$

d. Class IIb ($j = 1, K_1 = 1, K_2 = -2$) or class IIb' ($j = 1, K_1 = -1, K_2 = 2$)

Condition (16) becomes

$$\begin{aligned}
& [(p + \alpha)^2 + (q + \beta)^2]^{1/4} \\
& \times \tanh^{1/2}\{d[(p + \alpha)^2 + (q + \beta)^2]^{1/2}\} \\
& + [(p - 2\alpha)^2 + (q - 2\beta)^2]^{1/4} \\
& \times \tanh^{1/2}\{d[(p - 2\alpha)^2 + (q - 2\beta)^2]^{1/2}\} \\
& = 3 \tanh^{1/2}(d). \tag{34}
\end{aligned}$$

Within the new axes of symmetry $P = p\alpha + q\beta$ and $Q = -p\beta + q\alpha$ condition (16) becomes

$$\begin{aligned}
& [(P + 1)^2 + Q^2]^{1/4} \tanh^{1/2}\{d[(P + 1)^2 + Q^2]^{1/2}\} \\
& + [(P - 2)^2 + Q^2]^{1/4} \tanh^{1/2}\{d[(P - 2)^2 + Q^2]^{1/2}\} \\
& = 3 \tanh^{1/2}(d). \tag{35}
\end{aligned}$$

Similarly, in Fig. 4  we have

$$\mathbf{k}_1 = \mathbf{k}_2 + 3\mathbf{k}_{01} \quad \text{and} \quad \omega'_1 = \omega'_2 + 3\omega'_0, \tag{36}$$

with $\mathbf{k}_1 = (p + \alpha, q + \beta)$, $\mathbf{k}_2 = (p - 2\alpha, q - 2\beta)$, and $\mathbf{k}_{01} = \mathbf{k}^+_0 = (\alpha, \beta)$,

$$\omega'_1 = |\mathbf{k}_1|^{1/2} \tanh^{1/2}\{d[(p + \alpha)^2 + (q + \beta)^2]^{1/2}\}, \tag{37}$$


$$\omega'_2 = -|\mathbf{k}_2|^{1/2} \tanh^{1/2}\{d[(p - 2\alpha)^2 + (q - 2\beta)^2]^{1/2}\},$$


$$\omega'_0 = \tanh^{1/2}(d). \tag{38}$$

For $\theta = 90^\circ$, classes Ia and IIa are identical to classes Ib and IIb, respectively, and dissociate from each other as the angle θ decreases. From this dissociation it follows that each class is exclusive to one another since one cannot observe simultaneously for the same p and q two resonances of different classes involving a same basic wave harmonic \mathbf{k}_{0i} .

The instabilities arising as the wave steepness increases are detected by investigating the vicinity of the linear resonances in the (p, q) plane. The instabilities are computed with the numerical procedure presented in the appendix. The eigenproblem is described and the resolution and convergence of the numerical scheme is discussed.

3. Numerical results and discussion

IK94 and [Kimmoun et al. \(1999\)](#) have isolated three regimes of instability for three-dimensional waves in deep ocean. The first regime refers to progressive “long-crested waves” (for example $\theta = 80^\circ$, [Fig. 1](#) —left in IK94). While propagating in one direction they have long crests in the transverse direction compared to the wavelength of the propagating direction. Such waves look similar to progressive Stokes waves that have crests of infinite length. For weak wave steepness (approximately for $h < 0.20$), these waves are unstable to class Ia modulational instabilities: modulations of the wave train occur in the direction of propagation and groups appear while angle θ is kept unchanged. Like Stokes waves, it is likely that the unstable subharmonic mode that modulates the wave train might become dominant in the wave spectrum through probable input of energy from higher modes: this can lead to subharmonic transitions that make the wave train longer and longer after successive transitions, while higher modes could be dissipated quicker through viscous processes, that is, the frequency downshifting phenomenon. The process yielding to such transitions is not yet clear although some studies like that of [Skandrani et al. \(1996\)](#) found numerically that viscous damping might play a key role while taking into account viscosity, rotationality, and capillarity, but it is not the purpose of the present study to compute the time evolution of the fully nonlinear problem. For higher wave steepnesses the wave train is unstable to class IIa instabilities: these unstable modes are phase-locked with the wave train and are three-dimensional. They are illustrated in [Su \(1982\)](#) and in [Caulliez and Collard \(1997\)](#), that is, the horseshoe-patterned wave fields.

The second regime is the fully three-dimensional wave field (e.g., $\theta = 45^\circ$, [Fig. 1](#) —right in IK94). They are short-crested waves; that is, the wavelengths in both horizontal directions are of same order. For a very large range of the wave steepness (up to around $h = 0.6$) these waves are unstable to class Ib modulational instabilities, which are similar to class Ia

instabilities except that they change angle θ and modulation also occurs in the transverse direction. For very steep waves, class IIb instabilities dominate. These instabilities have a complex three-dimensional structure.

The third regime is close to the standing wave limit although they are still progressive and the wavelength in the direction of propagation is much longer than that of the transverse direction. These waves are unstable to class Ia instabilities, whatever the wave steepness. In this study we will keep in mind this parameter regime of instability and see how it can be perturbed when the flow becomes shallower.

The first step to locate the instabilities in the (p, q) wavenumber plane is to represent the instability diagrams in the linear approximation (for $h = 0$). They are plotted in long dashed lines in [Figs. 5–7](#) for $\theta = 80^\circ$, and they are the locations where the two perturbative modes are in resonance with each other; that is, for the respective frequencies the two modes involved coalesce through interaction with the basic wave, which provides two or three basic modes (at least quartet-resonances for class I and quintet-resonances for class II instabilities): when varying one parameter, the frequencies of the two perturbative modes are crossing through mutual exchange of energy via the basic wave and the coalescence gives rise to an instability. Once the linear interactions are known, we simply investigate numerically in the vicinity of the linear diagrams the “nonlinear” instability while the wave steepness (nonlinearity) increases. Nonlinearities create bands of instability. Their widths increase with the wave steepness in the vicinity of the linear diagrams as plotted in [Figs. 5–7](#). The classes of instability are identified by inspecting the eigenvectors corresponding to each eigenmode. The next step is to look numerically for the dominant instability within these bands for each class (the location of the maximum growth rate) and thus predict which (p, q) instability is more likely to appear first in the propagative motion. The bandwidths increase with the wave steepness.

For long-crested waves “close” to progressive Stokes waves (for $\theta = 80^\circ$), class Ia instability is no longer dominant earlier in h with the decreasing depth (e.g., [Fig. 8](#)), that is, at $h = 0.18$ for $d = 2$, $h = 0.15$ for $d = 1.5$, and at $h = 0.10$ for $d = 1$. This is in agreement with results of [Kimmoun et al. \(1999\)](#) who found this critical value to be around $h = 0.32$ for deep water. Class IIa horseshoe-patterned instability is still phase-locked with the basic wave for depths 2.0 and 1.5 (e.g., [Figs. 5–7](#)) but propagates at different frequency for $d = 1$; that is, the dominant class IIa instability does not propagate at zero frequency (note here that the eigenproblem is solved within the frame of reference moving with the basic wave). This class IIa instability is, however, not any more dominant in contrast to deep water for which it takes the lead around $h = 0.32$. For finite depth flow, class IIb instability becomes dominant beyond the above critical values for which class Ia stops dominating. This in turn generates a more complex three-dimensional flow composed of groups with no particular property like phase-locking.

In [Fig. 7](#) (bottom) note that the band of class IIa instability passes the axis of symmetry: this is due to interactions between the classes of instability. Another class of instability or a degeneracy repulses the band of instability of class IIa if a same perturbative harmonic is involved. The class IIa resonance corresponding to a coalesce of two eigenmodes is then delayed/reported elsewhere in the p - q plane. This process is generic in these wave-wave interactions and is broadly discussed in [Badulin et al. \(1995\)](#).

In [Fig. 9](#) growth rates for class I instabilities are represented: both classes present a restabilizing depth depending on the wave steepness for which these instabilities are neutrally stable. This can be seen as an extension of [Whitham’s \(1967\)](#) criterion, which predicted a restabilization of two-dimensional class I instability for Stokes waves at depth $d = 1.363$. Below this value [McLean \(1982b\)](#) found that class Ia instability becomes three-dimensional and increases exponentially with decreasing depth. The growth rates plotted in [Fig. 9](#) present a similar behavior where we observe a restabilization for both classes Ia and Ib, and then an exponential growth below a critical value of the depth depending on the wave steepness but also on the class of instability considered.

For fully three-dimensional short-crested waves (for $\theta = 40^\circ$), class Ib dominates down to depth $d = 1.5$ in accordance with results of IK94 and [Kimmoun et al. \(1999\)](#) for deep water. Below this value class Ia dominates, although there is a tendency for class IIa to take the lead around $h = 0.26$ with, however, a nonzero frequency (we did not find it useful to report the fastidious tables mentioning the frequencies of the unstable modes). For this range of three-dimensional waves, [Fig. 10](#) suggests that the value of the restabilizing depth is delayed (below $d = 1$) and occurs at weaker wave steepness for class Ib.

For progressive long-crested waves close to standing waves (for $\theta = 10^\circ$), class Ia dominates for depths $d = 2$ and $d = 1.5$. Below, these instabilities and those of class Ib decrease with depth, and the value of the restabilizing depth is delayed much below depth $d = 1$. In contrast, class IIa instability (not phase-locked with the basic wave train) grows with decreasing depth until taking the lead (e.g., at $h = 0.22$ for $d = 1$).

These results denote how drastically the depth parameter can change the parameter regime of three-dimensional water waves while they propagate toward the coast. This has already been mentioned by [Joualalen et al. \(1996\)](#), who found that very locally, such waves can be subject to strong superharmonic instabilities and thus the authors questioned their

observability. Their [Fig. 4](#) indicates that the growth rates are getting more and more important with decreasing depth, that is, of order h^4 for $d = 1$, h^2 for $d = 0.6$. As mentioned earlier, generally we have not been able to perform computations below $d = 1$. [Ioualalen et al. \(1996\)](#) found that for this value harmonic resonances have growth rates of order h^4 around $\theta = 65^\circ$. In such a parameter regime, [Fig. 7](#) (bottom) indicates that class IIb instabilities are of order h^3 . This indicates that, although harmonic resonances are strong compared to deep water, they are, however one order weaker than class IIb instabilities for the same wave field. This clearly denotes that finite depth short-crested waves can be observable as experimented by [Hammack et al. \(1989\)](#), at least down to depth $d \approx 1$, although the authors generated much shallower waves.

Experiments on shallow water short-crested waves have been performed by [Hammack et al. \(1989\)](#), who have generated cnoidal water waves rather than sinusoidal wave fields. For that reason a comparison with our predictions is not recommended because our calculations are not valid for very shallow water (say shallower than approximately $d = 0.5$). That would be necessary to replace our formulation by the Kadomtsev–Petviashvili equation and derive a numerical procedure similar to the one we have processed.

Besides the question of how modes interact within a short-crested wave field, the predictions derived from this study provide a framework for interpreting observations or initiating relevant experiments or numerical simulations. The overall propagations and their timescales that occur in such a wave field are provided, considering the wide parameter regime of these waves (depth d , angle θ , and wave steepness h , all of them varying continuously in their own limits).

Acknowledgments

The authors would like to acknowledge with thanks the Australian Research Council for their research grant, Cray Research Australia, Melbourne, and the Centre de Calcul pour la Recherche, Paris-Jussieu, for use of their respective Cray supercomputers. Finally, the authors have appreciated the comments of the two anonymous referees who contributed to a substantial improvement of the manuscript first draft.

REFERENCES

- Badulin, S. I., V. I. Shrira, C. Kharif, and M. Ioualalen, 1995: On two approaches to the problem of instability of short-crested water waves. *J. Fluid Mech.*, **303**, 297–326..
- Benjamin, T. B., and J. E. Feir, 1967: The disintegration of wave trains on deep water. *J. Fluid Mech.*, **27**, 417–430..
- Cauilliez, G., and F. Collard, 1997: Three-dimensional nonlinear evolution of water waves: Laboratory study. *Ann. Geophys.*, **15**, C569..
- Hammack, J., N. Sheffner, and H. Segur, 1989: Two-dimensional periodic waves in shallow water. *J. Fluid Mech.*, **209**, 567–589..
- Hsu, J. R. C., Y. Tsuchiya, and R. Silvester, 1979: Third approximation to short-crested waves. *J. Fluid Mech.*, **90**, 179–196..
- Ioualalen, M., and C. Kharif, 1993: Stability of three-dimensional progressive gravity waves on deep water to superharmonic disturbances. *Eur. J. Mech. B*, **12-3**, 401–414..
- and —, 1994: On the subharmonic instabilities of steady three-dimensional deep water waves. *J. Fluid Mech.*, **262**, 265–291..
- , A. J. Roberts, and C. Kharif, 1996: On the observability of finite depth short-crested water waves. *J. Fluid Mech.*, **322**, 1–19..
- Kimmoun, O., M. Ioualalen, and C. Kharif, 1999: Instabilities of steep short-crested surface waves in deep water. *Phys. Fluids*, **11**, 1679–1681..
- Mackay, R. S., and P. G. Saffman, 1986: Stability of water waves. *Proc. Roy. Soc. London*, **406**, 115–125..
- Marchant, T. R., and A. J. Roberts, 1987: Properties of short-crested waves in water of finite depth. *J. Aust. Math. Soc.*, **29B**, 103–125..
- McLean, J. W., 1982a: Instabilities of finite amplitude water waves. *J. Fluid Mech.*, **114**, 315–330..
- , 1982b: Instabilities of finite amplitude gravity waves on water of finite depth. *J. Fluid Mech.*, **114**, 331–341..
- Mercer, R. G., and A. J. Roberts, 1994: The form of standing waves on finite depth water. *Wave Motion*, **19**, 233–244..
- Phillips, O. M., 1960: On the dynamics of unsteady gravity waves of finite amplitudes. *J. Fluid Mech.*, **9**, 193–217..

Roberts, A. J., 1983: Highly nonlinear short-crested water waves. *J. Fluid Mech.*, **135**, 301–321..

Skandrani, C., C. Kharif, and J. Poitevin, 1996: Nonlinear evolution of water surface waves: The frequency down-shift phenomenon. *Contemp. Math.*, **200**, 157–171..

Su, M.-Y., 1982: Three-dimensional deep-water waves. Part 1. Experimental measurement of skew and symmetric wave patterns. *J. Fluid Mech.*, **124**, 73–108..

Whitham, G. B., 1967: Non-linear dispersion of water waves. *J. Fluid Mech.*, **27**, 399–412..

Zakharov, V. E., 1968: Stability of periodic waves of finite amplitude on the surface of a deep fluid. *J. Appl. Mech. Tech. Phys. (USSR)*, **2**, 190–194..

APPENDIX

4. Numerical Scheme

The numerical scheme is an extension to finite-depth fluid of the procedure developed by IK94. An optimization has also been performed. Once the series (14)–(15) are truncated up to the order M and N and the basic wave solutions given by Marchant and Roberts (1987) are obtained up to the 35th order in h and both substituted in surface conditions (11)–(13), the resolution of the perturbation equations leads to a generalized eigenvalue problem of the form $\mathbf{A}\mathbf{u} = i\sigma\mathbf{B}\mathbf{u}$, where σ is the set of eigenvalues to be computed together with the corresponding eigenvectors $\mathbf{u} = (a_{jk}, b_{jk})$; \mathbf{A} and \mathbf{B} are complex matrix functions of the basic flow and wavenumbers p and q . IK94 used both collocation and Galerkin methods to solve the eigenvalue problem, and they found the latter technique much more efficient because it dissociates explicitly the sampling of the collocation points and the order (M, N) of truncation of the eigenmodes. We have consequently employed the Galerkin method to solve the eigenproblem. Taking advantage of the periodicity of both basic wave solutions and eigenmodes, Eqs. (12)–(13) are numerically integrated over one spatial period in the two horizontal directions using fast Fourier transforms over a range of $\nu \times \mu$ points whose coordinates are $x_u = 2\pi u/(\alpha\nu)$, $u = 0, \dots, \nu - 1$ and $y_{\mathbf{v}} = 2\pi \mathbf{v}/(\beta\mu)$, $\mathbf{v} = 0, \dots, \mu - 1$. The following eigenproblem is obtained at $z = \bar{\eta}(x, y)$:

$$\begin{aligned} & \sum_{J=-M}^M \sum_{K=-N}^N F_{J-l, K-r} [E_{JK}^{(1)}] a_{JK} + \sum_{J=-M}^M \sum_{K=-N}^N F_{J-l, K-r} [G_{JK}^{(1)}] b_{JK} \\ & = i\sigma a_{lr}, \\ & \sum_{J=-M}^M \sum_{K=-N}^N F_{J-l, K-r} [E_{JK}^{(2)}] a_{JK} + \sum_{J=-M}^M \sum_{K=-N}^N F_{J-l, K-r} [G_{JK}^{(2)}] b_{JK} \\ & = i\sigma \sum_{J=-M}^M \sum_{K=-N}^N F_{J-l, K-r} [H_{JK}] b_{JK}, \end{aligned}$$

where

$$G_{JK}^{(1)} = \{[\bar{\phi}_x(p + J\alpha)i + \bar{\phi}_y(q + K\beta)i] \cosh[\kappa_{JK}(\bar{\eta} + d)] + \kappa_{JK} \sinh[\kappa_{JK}(\bar{\eta} + d)]\} \frac{1}{\cosh(\kappa_{JK}d)},$$

$$H_{JK} = \frac{\cosh[\kappa_{JK}(\bar{\eta} + d)]}{\cosh(\kappa_{JK}d)}.$$

The functions $F_{J-l, K-r}\{f_{JK}\} = \sum_{\nu=0}^{\nu-1} \sum_{\mu=0}^{\mu-1} \mathbf{u}_{\nu\mu} f_{JK} e^{i\alpha(J-l)x} e^{i\alpha(K-r)y}$ are computed using a two-dimensional fast Fourier transform. We take $l = -M, \dots, M$ and $r(l) = -N(l), \dots, N(l)$ (with a step of 2) such that r has the same parity as l so that the eigenproblem is of order $L = (2M + 1)(2N + 1) + \delta_{lr}$, where $\delta_{lr} = 1$ if l and r have the same parity and $\delta_{lr} = -1$ elsewhere. IK94 took independent value of r and l so that they obtained an eigenproblem of order $L = 2(2M + 1)(2N + 1)$. At the end, since only perturbations of the same $x - y$ parities can interact with the basic unperturbed wave considering their complete classification of instabilities, their problem is redundant. In practice eigenvalues corresponding to mixed-parity modes are neutrally stable, and all mixed-parity components of all eigenvectors vanish so that there is no interaction with the short-crested wave field.

[Table A1](#) displays the significant improvement in CPU computational time of the method on a Cray J90. For $h = 0.10$ convergence up to the seventh digit is obtained with $M = N = 15$ (up to the fifth digit for $h = 0.25$) and the present method uses a quarter of the CPU time required for the IK94 method. This is a substantial improvement since the procedure we use to localize and evaluate the dominant instability is sequential (one run initializes parameters of the next run). The numerical convergence procedure is such that ν and μ are increased until the Fourier coefficients have converged, that is, the surface wave is efficiently described, then the convergence of the eigenvalues σ is obtained by increasing M and N .

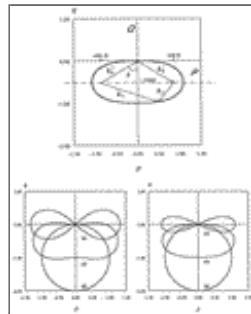
Tables

Table A1. Convergence of the eigenvalue (σ) associated to the dominant instability for class Ia, $\theta = 65^\circ$, $d = 1.5$: Comparison between IK94 method and the present one (IKR). Eigenvectors are also computed.

| $M = N$ | $(h = 0.1, p = 0.08, q = 0)$ | | $(h = 0.25, p = 0.26, q = 0)$ | | CPU (s) | |
|---------|------------------------------|----------------|-------------------------------|----------------|---------|-----|
| | $\tau(\sigma)$ | $-\Re(\sigma)$ | $\tau(\sigma)$ | $-\Re(\sigma)$ | IK94 | IKR |
| 7 | 0.4702481 (-1) | 0.7746467 (-3) | 0.4411487 | 0.2867638 (-2) | 51 | 42 |
| 9 | 0.4702492 (-1) | 0.7747131 (-3) | 0.4411721 | 0.2868229 (-2) | 103 | 61 |
| 11 | 0.4702492 (-1) | 0.7747109 (-3) | 0.4411812 | 0.2868372 (-2) | 231 | 94 |
| 13 | 0.4702492 (-1) | 0.7747099 (-3) | 0.4411797 | 0.2868316 (-2) | 517 | 150 |
| 15 | 0.4702492 (-1) | 0.7747095 (-3) | 0.4411788 | 0.2868315 (-2) | 1094 | 249 |
| 17 | 0.4702492 (-1) | 0.7747092 (-3) | 0.4411806 | 0.2868301 (-2) | | 417 |

[Click on thumbnail for full-sized image.](#)

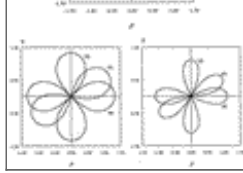
Figures



[Click on thumbnail for full-sized image.](#)

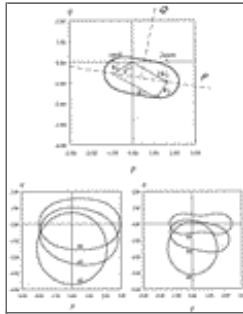
Fig. 1. Class Ia ($j = 1, K_1 = K_2 = 1$). Geometrical construction for depth $d = 0.5$ and angle $\theta = 60^\circ$ (top). Resonance diagrams obtained from the linear dispersion relation for angles $\theta = 0^\circ, 60^\circ, 90^\circ$ and depths (left) $d = 2$ and (right) $d = 0.5$.





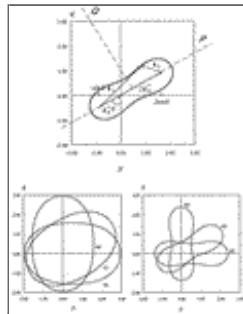
Click on thumbnail for full-sized image.

Fig. 2. Same as Fig. 1 but for class Ib ($j = 1, K_1 = 1, K_2 = -1$).



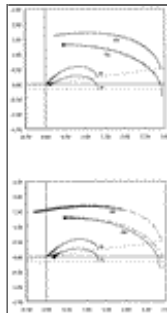
Click on thumbnail for full-sized image.

Fig. 3. Same as Fig. 1 but for class IIa ($j = 1, K_1 = 1, K_2 = 2$).



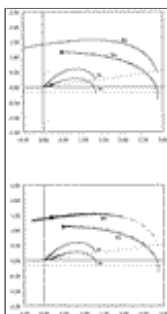
Click on thumbnail for full-sized image.

Fig. 4. Same as Fig. 1 but for class IIb ($j = 1, K_1 = 1, K_2 = -2$).



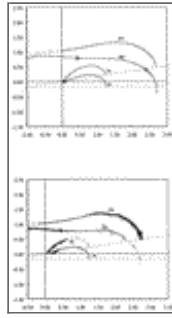
Click on thumbnail for full-sized image.

Fig. 5. Diagrams of instability for angle $\theta = 80^\circ$ and depth $d = 2.0$: (top) $h = 0.10$, (bottom) $h = 0.20$. Dashed lines correspond to axes of symmetry, dot-dashed lines correspond to linear resonance diagrams, crosses (\times) and circles (\odot) are locations of class IIa zero-frequency and maximum growth rate. Solid circles (\bullet) locate the overall dominant instability.



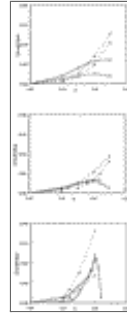
Click on thumbnail for full-sized image.

Fig. 6. Same as [Fig. 5](#) but for depth $d = 1.5$.



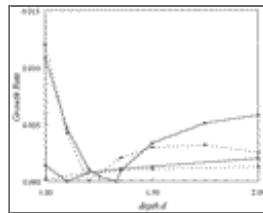
[Click on thumbnail for full-sized image.](#)

Fig. 7. Same as [Fig. 5](#) but for depth $d = 1.0$.



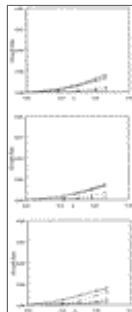
[Click on thumbnail for full-sized image.](#)

Fig. 8. Maxima of growth rates for angle $\theta = 80^\circ$ for depth $d = 2.0$ (top), depth $d = 1.5$ (middle) and depth $d = 1.0$ (bottom): (solid-open circle) class Ia, (solid-cross) class Ib, (dashed-open circle) class IIa, and (dashed-cross) class IIb.



[Click on thumbnail for full-sized image.](#)

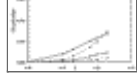
Fig. 9. Growth rate maxima for angle $\theta = 80^\circ$: (solid-open circle) class Ia, $h = 0.10$, (solid-cross) class Ia, $h = 0.20$, (dashed-open circle) class Ib, $h = 0.10$, and (dashed-cross) class Ib, $h = 0.20$.



[Click on thumbnail for full-sized image.](#)

Fig. 10. Same as [Fig. 8](#) for angle $\theta = 40^\circ$.





Click on thumbnail for full-sized image.

Fig. 11. Same as [Fig. 8](#) for angle $\theta = 10^\circ$.

Corresponding author address: Dr. Mansour Ioualalen, Centre IRD de Nouméa, BP A5, 98848 Nouméa Cedex, New Caledonia.

top ▲



© 2008 American Meteorological Society [Privacy Policy and Disclaimer](#)
Headquarters: 45 Beacon Street Boston, MA 02108-3693
DC Office: 1120 G Street, NW, Suite 800 Washington DC, 20005-3826
amsinfo@ametsoc.org Phone: 617-227-2425 Fax: 617-742-8718
[Allen Press, Inc.](#) assists in the online publication of *AMS* journals.